

possibly because of the inherent difficulty in the synthesis and control of stoichiometry of these materials. The Fe–S system has a complex phase diagram, with broad range of compositions of Fe_{1-x}S (pyrrhotite) phases^[7] occurring between FeS and FeS_2 , showing interesting magnetic^[8–10] and electrical properties.^[11] Fe_7S_8 is a well-defined phase in this region, showing ferrimagnetism with $T_N = 600$ K.^[9] We deemed it important to synthesize iron sulfide nanowires by virtue of their interesting chemistry and magnetic properties. In this communication, we report the first successful synthesis of semiconducting nanowires of Fe_{1-x}S ($x \approx 0.12, 0.09$), of which the $\text{Fe}_{0.88}\text{S}$ (Fe_7S_8) nanowires are ferrimagnetic, showing magnetic hysteresis at room temperature.

In order to synthesize Fe_{1-x}S nanowires, a hybrid composite (**I**) with ethylenediamine was first prepared by solvothermal procedure (see Experimental). Scanning electron microscopy (SEM) and transmission electron microscopy (TEM) images of the composite **I** showed the presence of a high yield of lengthy nanowires with diameters in the range of 80–150 nm and lengths of several micrometers as shown in Figure 1. The infrared (IR) spectrum showed characteristic peaks of the amine, although the bands due to C–N and N–H stretching frequencies were considerably shifted towards lower values due to the bound nature of the amine. Energy dispersive X-ray (EDX) analysis of several samples of **I** carried out over different regions of each sample gave an average Fe/S ratio of

Synthesis and Characterization of Magnetic Iron Sulfide Nanowires

By Manashi Nath, Amitava Choudhury, Asish Kundu, and C. N. R. Rao*

A variety of inorganic nanowires have been synthesized in the last three to four years.^[1] Among these, magnetic nanowires are of interest because of their potential applications in magnetic recording and other areas. Nanowires and nanorods of magnetic metals, such as Fe, Co, and Ni,^[2] and their alloys^[3] have been prepared by employing template-directed synthesis. Although there are reports of nanotubes, nanorods, and nanowires of several metal chalcogenides,^[4,5] oxides,^[6] and nitrides^[1,6] there is no report to date on iron sulfide nanowires,

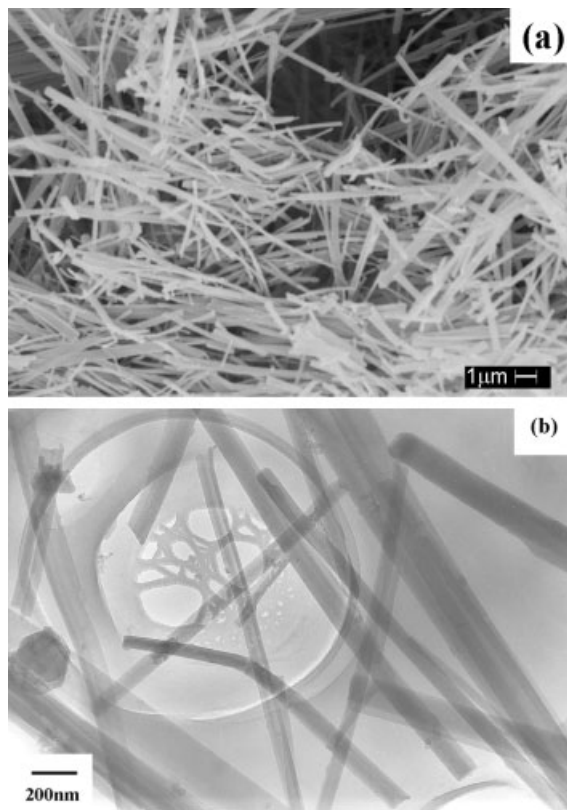


Fig. 1. a) SEM image of the organic–inorganic composite, $\text{Fe}_{1-x}\text{S}(\text{en})_{0.5}$, **I**. b) Low-magnification TEM image of composite **I**. Apart from nanowires, some layer-rolled kind of structures are also observed (as seen in the center of the image).

[*] Prof. C. N. R. Rao, M. Nath, Dr. A. Choudhury, A. Kundu
Chemistry and Physics of Materials Unit
Jawaharlal Nehru Center for Advanced Scientific Research
Jakkur P.O., Bangalore 560 064 (India)
E-mail: cnrrao@jncasr.ac.in

Prof. C. N. R. Rao, M. Nath, Dr. A. Choudhury
Solid State and Structural Chemistry Unit
Indian Institute of Science
Bangalore 560 012 (India)

~0.7–0.8:1. The C, H, N analysis of **I** gave the percentages to be 11.2462, 3.8355, and 11.9318 %, respectively, corresponding to the nominal formula, $\text{Fe}_{1-x}\text{S}(\text{en})_{0.5}$ ($x = 0.2\text{--}0.3$, en = ethylenediamine). Thermogravimetric analysis of **I** showed a sharp weight loss around 200 °C due to the loss of the amine bound to the metal center.^[12] The powder X-ray diffraction (XRD) pattern of **I** showed the presence of a low-angle line at $\sim 8^\circ$, in addition to broad, weak reflections. The low-angle line is similar to that found in many of the organic–inorganic composites of CdE and ZnE (E = S, Se) containing metal–chalcogen layers pillared by an amine.^[12,13] The nanowires of $\text{Fe}_{1-x}\text{S}(\text{en})_{0.5}$ were paramagnetic, showing insulating behavior at room temperature.

The amine in **I** could be removed partially under vacuum. It could, however, be removed completely by heating **I** to 200–300 °C under Ar flow (200 sccm, standard cubic centimeters per minute), yielding pure inorganic Fe_{1-x}S nanowires (see Experimental). IR spectra of **I** heated to 200 °C and 300 °C (designated as **II**, **III**, respectively) showed the absence of the peaks corresponding to the amine. The XRD patterns of **II** and **III** were characteristic of pyrrhotite phases (prominent lines at $d = 2.98, 2.63, 2.05, 1.72 \text{ \AA}$).^[14]

The SEM image of **II** in Figure 2a shows an abundant presence of nanowires with lengths of the order of micrometers. EDX analysis of individual nanowires revealed a Fe/S ratio of 0.88:1, indicating the composition to be Fe_7S_8 . Low-magnification TEM images of **II** (Fig. 2b) show the diameters to be in the range 40–180 nm. High-resolution TEM (HRTEM) images show the presence of different domains with interesting lattice fringes (Fig. 2c), but they all belong to the same crystallographic phase. The inset in A shows the simulated fast Fourier-transform (FFT) pattern obtained from the boxed region of the HRTEM image corresponding to a hexagonal close-packed (hcp) lattice with a hexagonal arrangement of the spots that can be indexed to the (204) plane of the 4C phase of Fe_7S_8 , ($a = 12.811, b = 6.870$, and $c = 11.885 \text{ \AA}$, $\beta = 117.17^\circ$, JCPDS file, card number: 29-0723). The layer spacing obtained from the lattice fringes from a different part of the image is $\sim 2.6 \text{ \AA}$, corresponding to $d(004)$ of 4C- Fe_7S_8 . The electron diffraction (ED) pattern in the inset in B shows spacings of 3.2, 2.6, and 1.7 Å due to the (202), (004), and (040) planes, respectively. The $d(004)$ spots in the ED pattern show splitting due to superstructures of Fe_7S_8 . 4C- Fe_7S_8 is known to be a stable, ordered phase at room temperature.^[7a]

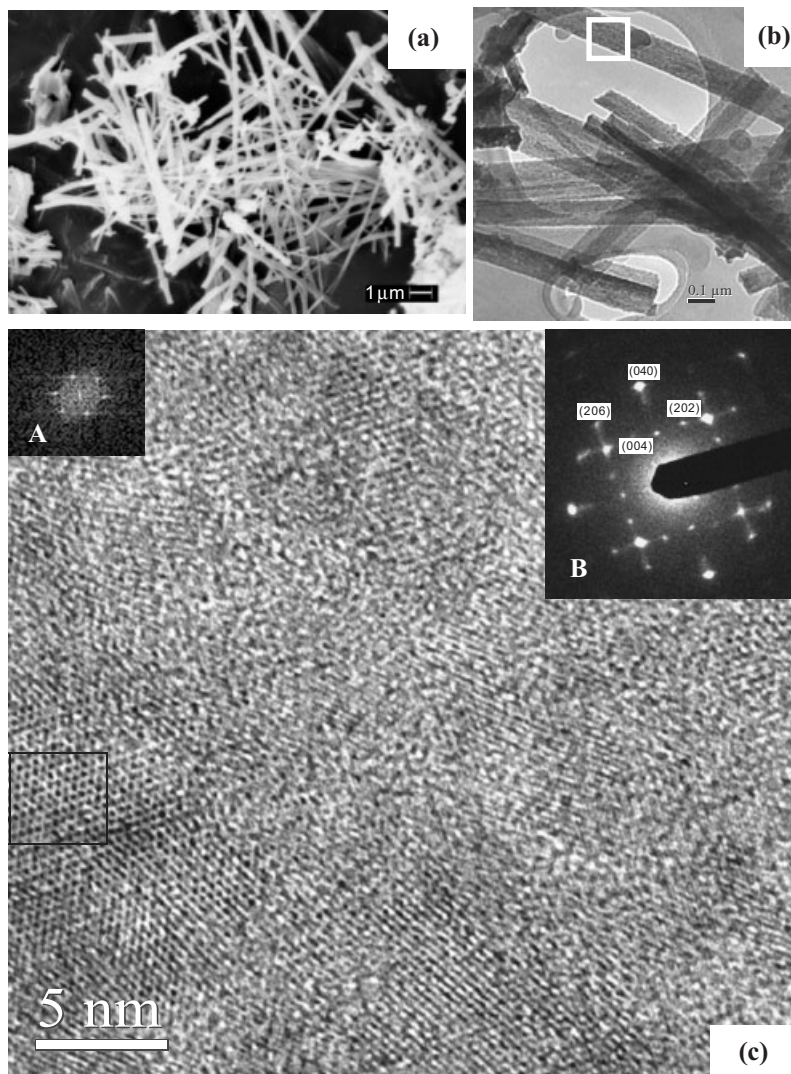


Fig. 2. a) SEM image of the 200 °C heat-treated product, **II**, showing a considerable yield of the nanowires. b) Low-magnification TEM image of the nanowires. Some nanowires are obtained in bundles. c) High-resolution image (HRTEM) of the nanowire from the boxed portion of the image in (b). Hexagonal arrangements seen in the bottom left portion of the image. The distance between the vertices of the hexagon was estimated to be 3.2 Å. The simulated FFT pattern from the boxed region in the image is shown in the inset in A, clearly showing the hexagonal arrangement of the spots. The inset in B shows the ED pattern obtained from this nanowire.

The SEM image of **III** in Figure 3a reveals the presence of a large proportion of nanowires. EDX analysis on these nanowires showed the composition to be Fe_{1-x}S with $x = 0.08\text{--}0.1$, showing that the amine composite heated at a higher temperature (300 °C) to be less Fe deficient. Low-magnification TEM images show the presence of short nanowires of 80–100 nm diameter in addition to rolled structures as can be seen from Figure 3b. The rolled structures are not nanotubes or scrolls, but are incompletely folded structures. The HRTEM image of the nanowires shows the lattice fringes marked by the presence of alternate dark and light strips, indicating the presence of a two-layer periodicity. The distance between two dark strips is $\sim 5.6 \text{ \AA}$, while that between the

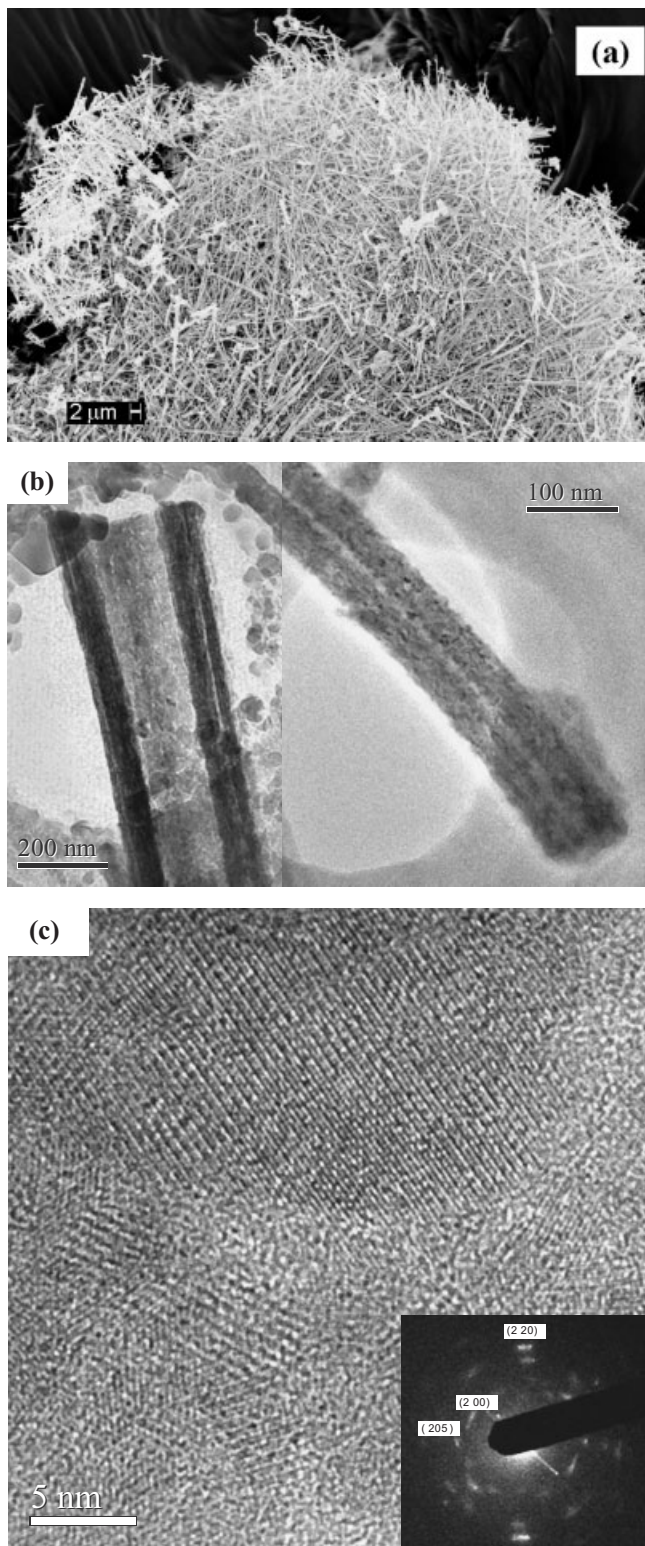


Fig. 3. a) SEM image of the 300 °C heat-treated product, **III**, showing a good yield of the nanowires. b) TEM image of **III** showing some incompletely rolled structures along with nanowires. c) HRTEM image of the nanowires showing periodic stacking of the layers in some region. The inset shows the ED pattern obtained from the nanowires.

light strips is $\sim 2.9 \text{ \AA}$, which correspond to the (102) and (200) planes of 5T- Fe_{1-x}S phase [JCPDS file, card number: 29-0724]. The ED pattern from the nanowires shows spots due to (200), (205), and (220) reflections of the 5T-pyrrhotite phase ($a = 6.888$ and $c = 28.670 \text{ \AA}$).

Most pyrrhotites exhibit some superstructures as a result of the Fe vacancy ordering, giving rise to varied magnetic and electrical properties and complex phase relations.^[7–11] The ordered structure of Fe_7S_8 that can be achieved by the maximum separation of iron vacancy sites is formed by the alternation of partially filled Kagome net layers with fully filled iron layers, i.e., there is an Fe vacancy in every alternate layer. The structure of Fe_{1-x}S ($x \approx 0.1$) is based on the Fe_7S_8 structure, where partially filled kagome net layers and iron filled layers are stacked in such a way that long-range order is established along the c -direction.

The temperature variation of the magnetic susceptibility of **II** (Fig. 4a) shows a ferrimagnetic behavior with a transition temperature of $\sim 600 \text{ K}$, characteristic of Fe_7S_8 .^[9] The Weiss-type behavior can be reversed upon cooling with a thermal hysteresis of 20–25 K. More importantly, nanowires, **II**, show a hysteresis loop at room temperature (297 K) (see

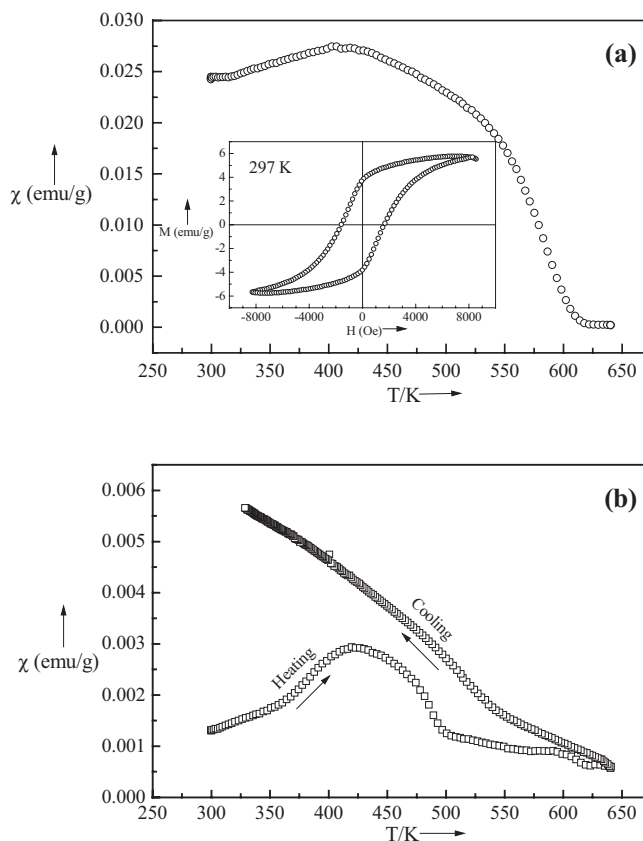


Fig. 4. a) The temperature variation of the magnetic susceptibility between 300–650 K of **II**. The inset shows the hysteresis loop obtained at 297 K. b) The temperature variation of the susceptibility between 300–650 K of **III** showing peak-type transition in the heating cycle.

inset of Fig. 4a). A saturation magnetization of 6 emu g^{-1} ($1 \text{ emu g}^{-1} = 1 \text{ A m}^2 \text{ kg}^{-1}$) is achieved with an applied field of 8000 Oe ($1 \text{ Oe} = 10^{-4} \text{ T}$). The remnant magnetization and coercivity are 4 emu g^{-1} and 2000 Oe, respectively. The magnetic susceptibility of the Fe_{1-x}S ($x = 0.08\text{--}0.1$) nanowires, **III**, on the other hand, is different from that of **II**. Nanowires of **III** show a lambda-type transition^[10] at 420 K in the high-temperature susceptibility data (Fig. 4b). Except in the narrow temperature range of 375–475 K, the ferrimagnetism disappears on either side and predominant antiferromagnetism becomes evident. The antiferromagnetic to paramagnetic transition occurs at 600 K. On cooling the sample, the peak disappears showing a Weiss-type behavior, a mixed behavior common in the Fe_{1-x}S phases.^[9] **III** does not exhibit a hysteresis loop at room temperature and the magnetization is at least one order of magnitude smaller than that of **II**, indicating predominant antiferromagnetic interactions. We must point out that the magnetic properties reported here represent the average behavior of a bundle of nanowires. It has not been possible to strictly compare the observed properties with those of the bulk, since the literature reports on the bulk properties vary rather widely. Electrical resistivity measurements on pressed pellets of Fe_7S_8 and Fe_{1-x}S nanowires show semiconducting behavior at room temperature and below.

In conclusion, we have been successful in developing a one-step synthesis to produce iron sulfide nanowires of well-defined compositions in high yields. The isolation and characterization of magnetic Fe_7S_8 nanowires are noteworthy.

Experimental

The synthesis procedure of Fe_{1-x}S nanowires comprises two steps. In the first step, solvothermal methods have been employed to obtain an organic–inorganic composite (**I**), $\text{Fe}_{1-x}\text{S}(\text{en})_{0.5}$. The amine removal from this composite by heating under a flow of Ar at 200–300 °C yielded nanowires of Fe_{1-x}S .

Preparation of the Organic–Inorganic Composite, I: In a typical synthesis procedure, $\text{FeCl}_2 \cdot 4\text{H}_2\text{O}$ (0.2982 g, 1.5 mmol) was mixed with CH_3CSNH_2 (thioacetamide, 0.2254 g, 3 mmol) in a Teflon-lined steel autoclave (23 ml capacity) and 10 mL ethylenediamine was added to it. The container was sealed and heated to 180 °C for 4 days under solvothermal conditions. A purple-blackish wool-like flocculate was obtained, which was immediately sonicated in methanol, filtered, washed with methanol, and dried in vacuum. It should be noted that the as-synthesized product is always stored under vacuum as longer exposure to air under ambient conditions leads to conversion of the iron-sulfide phases to the oxide/hydroxide phases. For this reason, after opening the autoclave, sonication and filtration were carried out in minimum time.

Synthesis of Fe_7S_8 (II) and Fe_{1-x}S (III) Nanowires by Amine Removal from the Composite I: The composite **I** was taken in a quartz boat and placed inside a quartz tube, which was put in a horizontal tubular furnace. The sample was heated under a flow of Ar (200 sccm) to 200–300 °C and kept at that temperature for 20–30 min. The furnace temperature was allowed to come down to room temperature naturally before taking out the product. The color of the reactant powder changed to black after the thermal treatment. Fe_7S_8 nanowires (**II**) were obtained at 200 °C, while at 300 °C, Fe_{1-x}S ($x = 0.08\text{--}0.1$) nanowires (**III**) were produced.

Characterization: The samples were characterized by powder XRD (Seifert 3000TT), SEM (Leica S440i fitted with Leo software for EDX analysis), TEM (JEOL JEM 3010, operating at 300 kV), IR spectroscopy (Bruker IFS-66v/S). Magnetic measurements were carried out using a VSM (LakeShore) and by the Faraday technique (Lewis Coil force magnetometer, George Associates).

Received: August 19, 2003
Final version: October 4, 2003

- [1] a) J. Hu, T. Wang Odom, C. M. Leiber, *Acc. Chem. Res.* **1999**, 32, 435. b) Y. Xia, P. Yang, Y. Sun, Y. Wu, B. Mayers, B. Gates, Y. Yin, F. Kim, H. Yan, *Adv. Mater.* **2003**, 15, 353.
- [2] a) T. Thurn-Albrecht, J. Schotter, G. A. Kästle, N. Emley, T. Shibauchi, L. Krusin-Elbaum, K. Guarini, C. T. Black, M. T. Touminen, T. P. Russell, *Science* **2000**, 290, 2126. b) J. Bao, C. Tie, Z. Xu, Q. Zhou, D. Shen, Q. Ma, *Adv. Mater.* **2001**, 13, 1631. c) S. Liu, J. Zhu, Y. Matsai, I. Felner, A. Gedanken, *Chem. Mater.* **2000**, 12, 2205. d) L. Sun, P. C. Searson, C. L. Chien, *Appl. Phys. Lett.* **2001**, 79, 4429.
- [3] a) J. P. Pierce, E. W. Plummer, J. Shen, *Appl. Phys. Lett.* **2002**, 81, 1890. b) Z. Zhang, D. A. Blom, Z. Gai, J. R. Thompson, J. Shen, S. Dai, *J. Am. Chem. Soc.* **2003**, 125, 7528. c) Y.-G. Guo, L.-J. Wan, C.-F. Zhu, D.-L. Yang, D.-M. Chen, C.-L. Bai, *Chem. Mater.* **2003**, 15, 664.
- [4] a) R. Tenne, L. Margulis, M. Genut, G. Hodes, *Nature* **1992**, 360, 444. b) L. Margulis, G. Salitra, R. Tenne, *Nature* **1993**, 365, 113. c) R. Tenne, *Chem. Eur. J.* **2002**, 8, 5303.
- [5] a) M. Nath, C. N. R. Rao, *J. Am. Chem. Soc.* **2001**, 123, 4841. b) M. Nath, C. N. R. Rao, *Angew. Chem. Int. Ed.* **2002**, 41, 3451. c) C. N. R. Rao, M. Nath, *J. Chem. Soc. Dalton Trans.* **2003**, 1.
- [6] P. Yang, Y. Wu, R. Fan, *J. Nanosci. Nanotechnol.* **2002**, 1, 1.
- [7] a) H. Nakazawa, N. Morimoto, *Mater. Res. Bull.* **1971**, 6, 345. b) C. N. R. Rao, K. P. R. Pisharody, *Prog. Solid State Chem.* **1976**, 10, 207. c) J. C. Ward, *Rev. Pure Appl. Chem.* **1970**, 20, 175.
- [8] a) J. L. Horwood, M. G. Townsend, A. H. Webster, *J. Solid State Chem.* **1976**, 17, 35. b) V. H. Haraldsen, *Z. Anorg. Allg. Chem.* **1937**, 231, 78. c) E. Hirahara, M. Murakami, *Phys. Chem. Solids* **1958**, 7, 281.
- [9] F. Li, H. F. Franzen, *J. Solid State Chem.* **1996**, 126, 108.
- [10] T. Hirone, S. Maeda, N. Tsuya, *J. Phys. Soc. Jpn.* **1954**, 9, 736.
- [11] a) J. M. D. Coey, H. Roux-Buisson, R. Brusetti, *J. Phys. (Paris)* **1976**, 37, C4-1. b) M. G. Townsend, J. R. Gosselin, R. J. Tremblay, A. H. Webster, *J. Phys. (Paris)* **1976**, 37, C4-11. c) J. R. Gosselin, M. G. Townsend, R. J. Tremblay, *Solid State Commun.* **1976**, 19, 799.
- [12] X. Ouyang, T.-Y. Tsai, D.-H. Chen, Q.-J. Huang, W.-H. Cheng, A. Clearfield, *Chem. Commun.* **2003**, 2886.
- [13] a) X. Huang, J. Li, *J. Am. Chem. Soc.* **2000**, 122, 8789. b) Z.-X. Deng, L. Li, Y. Li, *Inorg. Chem.* **2003**, 42, 2331.
- [14] JCPDS (Joint Committee on Powder Diffraction Standards) files-International Center for Diffraction Data **1997**.